Formation of rotation-induced superlattices and their observation by tunneling spectroscopy

A. C. Seabaugh, Y.-C. Kao, H.-Y. Liu, J. H. Luscombe, H.-L. Tsai, M. A. Reed, and W. R. Frensley
Texas Instruments Incorporated, Central Research Laboratories, Dallas, Texas 75265

(Received 10 October 1990; accepted for publication 23 May 1991)

We show that superlattices can be formed in the ternary and quaternary In(GaAl)As alloys on InP by molecular beam epitaxy without mechanical shuttering. Periodic ordering is produced by rotation of the substrate through the naturally nonuniform distribution of beam fluxes at the rotating substrate. The growth rate and substrate rotation rate together determine the superlattice period which is measured by transmission electron microscopy and x-ray diffraction. Tunneling density-of-states measurements on resonant tunneling diodes, interpreted by a one-dimensional theoretical calculation of the miniband-structure, reveal the electrical properties of the superlattice.

In this letter we demonstrate an alternative method by which superlattices can be grown by molecular beam epitaxy (MBE) without mechanically shuttering the effusion sources. Shuttering techniques have numerous drawbacks including impurity generation problems and unreliability, particularly due to mechanical failure such as sticking which breaks the superlattice periodicity, obscures or destroys the desired transport property, and is not easily detected even after device fabrication. We show that a superlattice can be formed by an alternative method, i.e., by substrate rotation through the naturally asymmetric beam profiles in MBE growth chambers. The growth can be engineered to produce band discontinuities sufficient to cause conductance modulation even at room temperature.

In the growth of $In_{0.53}Ga_{0.47}As$ the Ga and In beam profiles at the wafer surface are naturally symmetric. In rotating the substrate, a strained-layer superlattice (SL) is formed with a period equal to the layer thickness grown per substrate revolution. A rotation-induced superlattice is thereby created without mechanical shuttering.

The growth system used is a Riber-2300 with indium-free mounting (5-cm-diam substrates) using conventional thermal group III and As_4 sources.[1] During growth, the center of the wafer is intentionally tilted away from the beam's focus-point by 5°. Typical substrate rotation speeds are between 2 and 5 rpm.

At constant growth rate the SL period is controlled by setting the substrate rotation speed. This is shown in Fig. 1 which is a transmission electron micrograph of a SL/resonant tunneling diode (RTD)/SL structure where the rotation speed was doubled with the initiation of the RTD double-barrier growth. The doubling of the rotation speed results in a halving of the SL period which can be seen in Fig. 1. The layers for the central RTD double barrier of Fig. 1 are $AlAs/In_{0.53}Ga_{0.47}As/InAs/In_{0.53}Ga_{0.47}As/AlAs$ with nominal thicknesses of 2/1/2/1/2 nm. The two light regions in the micrograph are the pseudomorphic AlAs tunneling barriers. On either side of the tunnel barriers is the strained-layer $In_xGa_{1-x}As/In_yGa_{1-y}As$ rotation-induced superlattice with average composition of $In_{0.53}Ga_{0.47}As$. X-ray diffraction measurements on this same sample confirm the presence of the SL satellite peaks and show that the ordering apparent in the transmission electron microscopy (TEM) micrographs is not an artifact of the sample preparation.

The SL is manifested electrically by a differential conductance oscillation in the RTD current-voltage (I-V) characteristic which is observable even at room temperature.[2] A typical conductance oscillation prior to the resonant tunneling current peak is shown in the I-V and dI/dV-V characteristics of an $In_{0.53}Ga_{0.47}As/AlAs$ RTD of Fig. 2. The $In_xGa_{1-x}As/In_yGa_{1-y}As$ SL in this device is also strained about the lattice-matched $In_{0.53}Ga_{0.47}As$ composition with a period as measured by x-ray diffraction of 5.7 nm. The complete structure consists of 0.5 μm ($\sim$87 periods) InGaAs SL uniformly doped to 5×10^{18} cm^{-3}, 0.2 μm ($\sim$35 periods) InGaAs SL doped to 1×10^{18} cm^{-3}, a 2/4.5/2 nm AlAs/InGaAs/AlAs resonant tun-

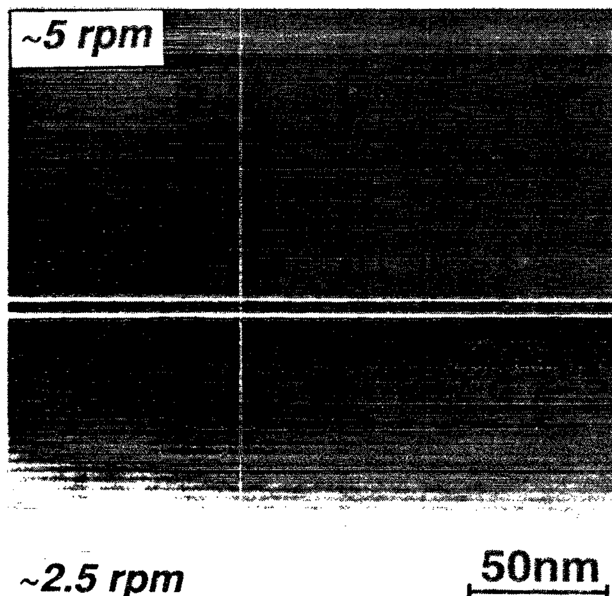

FIG. 1. Transmission electron micrograph of an $In_xGa_{1-x}As/In_yGa_{1-y}As$ rotation-induced superlattice showing the halving of the SL period with a doubling of the substrate rotation rate.

Downloaded 01 Feb 2005 to 130.132.120.180. Redistribution subject to AIP license or copyright, see http://apl.aip.org/apl/copyright.jsp

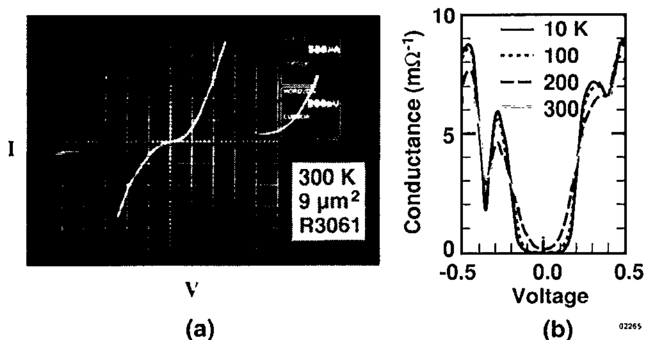

FIG. 2. Transport characteristics of an InGaAs/AlAs resonant tunneling diode: (1) room-temperature current-voltage measurement and (b) temperature dependence of the differential conductance, dI/dV.

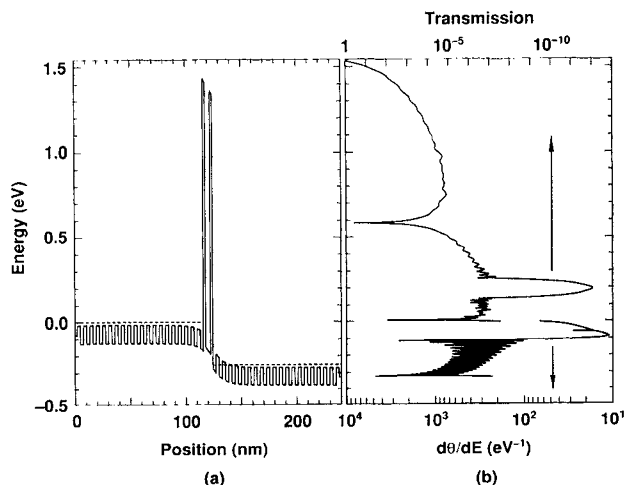

FIG. 3. (a) Calculated energy band diagram and (b) transmission coefficient for the InGaAs/AlAs rotation-induced SL RTD of Fig. 2, with a 20 layer, 5.7 nm period finite SL of $In_{0.43}Ga_{0.57}As/In_{0.63}Ga_{0.37}As$ in the emitter and collector regions of the RTD at a bias of 0.25 V. The dashed lines indicate the quasi-Fermi level positions in the emitter and collector. The transmission coefficient is computed for energies exceeding the conduction-band edge in the emitter; below this energy resonances are detected by plotting the change in phase of the reflection coefficient with energy.

neling double-barrier clad by 1.5 nm undoped InGaAs spacer layers, 0.2 μm InGaAs SL doped to 1×10^{18} cm^{-3}, and finally 0.2 μm InGaAs SL doped to 5×10^{18} cm^{-3}. For the electrical measurements, nonalloyed ohmic contacts were made to the emitter and collector ends of wet chemically etched mesa device structures.

In Fig. 2(a), the fundamental resonances through the first quantum well state are present at ±0.5 V; in agreement with our self-consistent calculations of the electrostatic band profile (described later). At roughly ±0.28 V, however, a decrease in the conductance of the device is observed which is particularly apparent for the negative bias polarity of Fig. 2(a). Measurements of the differential conductance, dI/dV, for this device are shown in Fig. 2(b) for the voltage range prior to the onset of the fundamental RTD resonance. The conductance extremes near ±0.28 V are observed to strengthen with decreasing temperature which is consistent with a resonant tunneling phenomenon.

The electrical properties of the SL can be inferred from the I-V characteristics of the RTD. We modeled the device based on the known RTD layer structure: a 20 period square-well SL in the emitter and collector layers with a 5.7 nm SL period as measured by x-ray diffraction. An $In_{0.43}Ga_{0.57}As/In_{0.63}Ga_{0.37}As$ SL compositional was assumed as a reasonable first estimate based on our ability to observe the SL by transmission electron microscopy. Shown in Figs. 3(a) and 3(b) are the (a) self-consistent calculation of the energy band profile and (b) transmission coefficient of the RTD structure under 0.25 V bias, i.e., the voltage at which the minigap in the collector is energetically aligned with the emitter electron distribution.

This calculation is obtained numerically by solution of a discretized Poisson–Thomas–Fermi equation[3] with a mesh size of 0.15 nm. The quantum mechanical transmission resonances, Fig. 3(b), for this potential profile are then computed from a self-consistent solution of the Schrödinger equation in the envelope approximation. For energies beneath the emitter band edge, miniband states are detected as resonances in the phase of the reflection coefficient for plane waves incident from the collector side.

In Fig. 3(a), the computed energy band diagram of the RTD is shown for a bias corresponding to the expected conductance minimum. For this bias, 0.25 V, the resonant transmission through the structure is suppressed due to the energetic alignment of the collector minigap with the electrons in the first miniband in the emitter. The computed value of 0.25 V is in reasonable agreement with the experimental value (Fig. 2) of roughly 0.35 V. In Fig. 3(b), the $n=1$ and $n=2$ transmission resonances are apparent at approximately 0.01 and 0.59 eV, respectively. A second minigap is observed in the energy range between 0.14 and 0.25 eV, respectively, which corresponds to the first minigap in the emitter. Analogous density-of-states tunneling effects have been previously observed in SL/single-barrier structures.[4,5]

These conductance oscillations are not related to the formation of a two-dimensional (2d) gas accumulation layer at the emitter side of the resonant tunneling double barrier. Multiple resonances would then occur between 2d states in the accumulation layer and 2d states in the quantum well. The 1.5 nm spacer layers and heavily doped emitter layer do not result in a sufficiently deep triangular potential well in the emitter accumulation region to support this mechanism. In addition, the conductance oscillation does not shift with magnetic field (9 T, applied in the direction of current flow) as would be expected if the oscillation were due to an accumulation region resonance.

The SL band structure and its dependence on composition and well shape were obtained from solutions of Schrödinger's equation in one dimension with a continuously varying effective mass,

$$\frac{-\hbar^2}{2}\frac{d}{dz}\left(\frac{1}{M(z)}\frac{d\psi}{dz}\right)+V(z)\psi(z)=E\psi(z), \qquad (1)$$

satisfying the Bloch condition $\Psi(z+a)=e^{ika}\Psi(z)$, where a is the periodicity of the potential and the effective

Downloaded 01 Feb 2005 to 130.132.120.180. Redistribution subject to AIP license or copyright, see http://apl.aip.org/apl/copyright.jsp

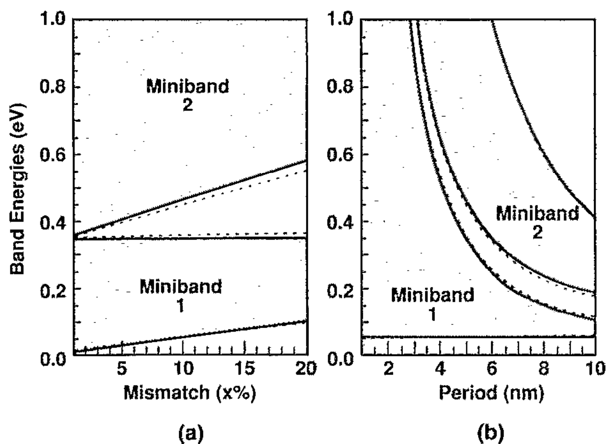

FIG. 4. One-dimensional miniband calculations: (a) miniband energy as a function of alloy mismatch x where x is defined for a SL with composition $In_{0.53+x}Ga_{0.47-x}As/In_{0.53-x}Ga_{0.47+x}As$ and a period of 5 nm, and (b) first and second miniband energies for a SL with a composition of $In_{0.43}Ga_{0.57}As/In_{0.63}Ga_{0.47}As$ as a function of SL period. Solid lines denote results for square-well potentials and dashed lines are results for a cosinusoidal-well potential.

mass, $V(z)=V(z+a)$, and $M(z)=M(z+a)$. Both V and M were obtained from the assumed periodic variations in the In concentration. The conduction-band offset was assumed to be 65% of the energy band-gap discontinuity between the $In_xGa_{1-x}As/In_yGa_{1-y}As$ SL layers. In the absence of experimental data, the fraction 65% was chosen as a compromise between the measured value of 62% for the AlGaAs/GaAs heterojunction[6] and the measured value of 71% for the $In_{0.52}Al_{0.48}As/In_{0.53}Ga_{0.47}As$ heterojunction.[7] The room-temperature energy band gap as a function of InAs mole fraction x was taken to be $E_g(x)=1.424-1.382x+0.318x^2$ after Aliev and Khalilov[8] modified to utilize Blakemore's value for the GaAs band gap[9] and the Casey and Panish value for the InAs band gap.[10] For the electron effective mass variation a linear interpolation between the values for GaAs and InAs was used also from Refs. 9 and 10, respectively.

The effect of alloy mismatch on the band structure is shown in Fig. 4(a) for a square-well potential, i.e., equal barriers and wells (solid lines). The SL is assumed to have a composition, deviating about the lattice-matched condition, of $In_{0.53+x}Ga_{0.47-x}As/In_{0.53-x}Ga_{0.47+x}As$ with a period of 5 nm. The value of x is defined as the alloy mismatch. The first two minibands in Fig. 4 (a) are separated by a minigap which increases with the alloy mismatch, x. The zero in energy is taken as the bulk conduction-band minimum for the InGaAs layer. Following the discussion of the last section we expect the onset of the conductance modulation to occur at an energy where the collector minigap becomes coenergetic with the bottom of the first emitter miniband. From this calculation, the position of the lower energy edge of the first minigap is only weakly dependent on the alloy mismatch, and thus the voltage at which the conductance oscillation is observed should not be strongly dependent on the SL composition. The minigap increases with alloy composition so the strength of the conductance modulation should depend on the alloy mismatch. The miniband structure is most strongly dependent on the SL period as can be seen in Fig. 4(b) where the first two minibands are computed for an alloy mismatch of 10%.

Also shown in Figs. 4(a) and 4(b) are the miniband structures computed for cosinusoidal potential oscillations (dashed lines) and their dependence on alloy mismatch and SL period. As can be seen, the cosinusoidal potential barrier produces only slight variations in the miniband structure relative to the square well potential. This is not surprising since the first Fourier component of the square well potential is a cosine function. The square well potential (Fig. 3) captures the essential physics of this system, and precise knowledge of the well shape introduces only a second-order correction.

In conclusion, a method for forming superlattices by MBE without mechanical shuttering is proposed and demonstrated. Superlattice were formed by substrate rotation through the naturally asymmetric beam profiles of MBE with sufficient band discontinuities to be observable at room temperature in device characteristics. Since these superlattices are a natural consequence of MBE growth of ternary and quaternary alloy, this work reveals an unintentional artifact which may be observed in hot electron and quantum devices formed by MBE.

The authors express appreciation for the excellent technical assistance of P. Stickney, R. Thomason, B. Garmon, and R. Aldert. This work was supported in part by ONR/DARPA contract No. N00014-87-C-0363 and WL contract No. F33615-89-C-1074.

[1] Y.-C. Kao, A. C. Seabaugh, H.-Y. Liu, T. S. Kim, M. A. Reed, P. Saunier, B. Bayraktaroglu, and W. M. Duncan, Proceedings of the 1st InP and Related Materials Conference, SPIE **1144**, 30 (1989).
[2] A. C. Seabaugh, Y.-C. Kao, H.-Y. Liu, J. H. Luscombe, H.-L. Tsai, M. A. Reed, B. E. Gnade, and W. R. Frensley, *Second International Conference on InP and Related Materials* (IEEE, New York, 1990), p. 416.
[3] J. H. Luscombe and W. R. Frensley, Nanotechnology **1**, 131 (1990).
[4] P. England, J. R. Hayes, J. P. Harbison, D. M. Hwang, and L. T. Florenz, Appl. Phys. Lett. **53**, 391 (1988).
[5] R. J. Aggarwal, M. A. Reed, W. R. Frensley, Y.-C. Kao, and J. H. Luscombe, Appl. Phys. Lett. **57**, 797 (1990).
[6] M. O. Watanabe, J. Yoshida, M. Mashita, T. Nakanisi, and A. Hojo, J. Appl. Phys. **57**, 5340 (1985).
[7] R. People, K. W. Wecht, K. Alavi, and A. Y. Cho, Appl. Phys. Lett. **43**, 118 (1983).
[8] M. I. Aliev and Kh. A. Khalilov, Dokl. Akad. Nauk Az. SSR **40**, 20 (1984).
[9] J. S. Blakemore, J. Appl. Phys. **53**, R123 (1985).
[10] H. C. Casey and M. P. Panish, *Heterostructure Lasers Part B* (Academic, New York, 1978).

Downloaded 01 Feb 2005 to 130.132.120.180. Redistribution subject to AIP license or copyright, see http://apl.aip.org/apl/copyright.jsp